Three-Dimensional, Two-Phase, Transonic, Canted Nozzle Flows

I-Shih Chang*
The Aerospace Corporation, El Segundo, California

A time-dependent numerical scheme, in conjunction with a three-dimensional, body-fitted, coordinate transformation technique, is utilized for the solution of subsonic-transonic-supersonic flows—both gas-only, one-phase, and fully coupled, gas-particle, two-phase—inside three-dimensional canted nozzles of arbitrary configurations. No difficulty is encountered with the time-dependent formulation for the solution of mixed transonic flowfield, which has been a bottleneck in many three-dimensional nozzle flow studies. Precise interpretation of flow variables in a canted nozzle is obtained through the simultaneous solution of multiple flow regions for motor aft closure and nozzle with two different coordinate centerlines. The results of the three-dimensional flow analysis are in good agreement with available test data.

Nomenclature

A_j = dimensionless friction term, Eq. (2)
a = exponent in the viscosity-temperature, Eq. (7)
B_j = dimensionless energy exchange term, Eq. (3)
C_D = particle drag coefficient
$\bar{C}_j$ = particle heat capacity
$\bar{C}_p$ = gas specific heat at constant pressure
$\boldsymbol{D,E,F,G,H}$ = vectors, Eq. (1)
D,E,F,G,H = vectors, Eq. (8)
e = dimensionless gas total energy per unit volume
f_j = momentum transfer parameter, Eq. (4)
g_c, g_r = convective and radiative parameters, Eq. (3)
h_j = dimensionless particle total energy per unit volume
$\bar{L}$ = reference length scale, e.g., unit foot (ft) or unit meter (m)
M = gas-phase Mach number
$\bar{m}_j$ = particle mass density
N = index: $N = 1$, one-phase flow; $N = 2$, two-phase flow
Nu_j = particle Nusselt number
P_r = gas-phase Prandtl number
p = dimensionless pressure
q, q_j = dimensionless gas, particle speed
Re_j = particle Reynolds number
$\bar{r}_j$ = particle radius
T, T_j = dimensionless gas, particle temperature
t = dimensionless time, $= \bar{V}_{\max 1}\,\bar{t}/\bar{L}$
$\bar{t}$ = time, s
u, v, w = dimensionless gas-phase velocity component along x, r, θ directions, respectively
u_j, v_j, w_j = dimensionless particle-phase velocity component along x, r, θ directions, respectively
$\bar{V}_{\max 1}$ = adiabatic maximum speed evaluated at the inlet plane
x, r, θ = dimensionless cylindrical coordinates
x, y, z = dimensionless rectangular coordinates
α_{ij} = direction cosines, Eq. (11)
β = nozzle canting angle
γ = gas specific heats ratio
δ = index: $\delta = 0$, rectangular coordinates; $\delta = 1$, cylindrical coordinates
ϵ, ϵ_j = gas accommodation coefficient and particle emissivity, respectively
ζ, ξ, η = transformed dimensionless coordinates
λ_q, λ_T = velocity lag, q_j/q; temperature ratio, T/T_j
$\bar{\mu}$ = micron, 10^{-6} m
$\bar{\mu}_g, \bar{\mu}_{t1}$ = gas viscosity at local and stagnation state, respectively
ρ, ρ_j = dimensionless gas; particle density
$\bar{\sigma}$ = Stefan-Boltzmann constant
τ = $(\gamma - 1)/(2\gamma)$
ϕ = particle mass fraction
ω = $\bar{C}_j/\bar{C}_p$

Superscript

$-$ = dimensioned quantity

Subscripts

g = gas-phase
j = particle-phase
max1 = adiabatic maximum state evaluated at the inlet plane
$t1$ = stagnation state evaluated at the inlet plane
1 = motor coordinates
2 = nozzle coordinates

I. Introduction

FOR many years, the Titan III 120-in.-diam, five-segment solid rocket motor (SRM) (SRM1205) has been a very reliable booster for delivering large payloads into space for various missions. An enhanced version of the motor is the five and one-half-segment motor (T34D SRM), which included an additional half-cylindrical segment near the forward closure. More recently, a seven-segment Titan IV SRM is being developed to meet ever-increasing payload demand. This is an improved version of the seven-segment motor (SRM1207) statically tested in 1969 for the Manned Orbiting Laboratory (MOL) program. Figure 1 illustrates the nonaxisymmetric motor aft closure geometry and canted nozzle design for the Titan IV SRM. The nozzle is canted 6 deg from bottom dead center (BDC) toward top dead center (TDC) to provide a thrust vector that intersects the central liquid-fueled core vehicle at its center of gravity.

As a result of application of asymmetric nozzle configurations in industry, three-dimensional nozzle analysis has re-

Received Jan. 30, 1988; revision received May 4, 1989.

*Engineering Specialist, Vehicle and Control Systems Division. Member AIAA.

ceived great attention. Reference 1 lists some recent developments in this area for a gas-only, one-phase flow inside three-dimensional nozzles. Gas-particle, two-phase flows inside rocket nozzles were studied in Refs. 2 through 7 in one-dimensional or two-dimensional spaces. Reference 8 solved three-dimensional, two-phase flows inside the supersonic portion of nozzles. However, a comprehensive gas-particle, two-phase, subsonic-transonic flow inside a three-dimensional canted nozzle has yet to be addressed in the literature. The transonic flow solution is recognized in industry as a bottleneck in many three-dimensional nozzle flow studies.

In this paper, a time-dependent numerical scheme in conjunction with the three-dimensional, body-fitted, coordinate transformation technique of Refs. 9 and 10 is utilized for the solution of gas-only, one-phase, and fully coupled, gas-particle, two-phase subsonic-transonic-supersonic flows inside three-dimensional nozzles of arbitrary configuration. No difficulty is encountered with the time-dependent formulation for the transonic nozzle flow field solution. Detailed results of the calculation are presented for the Titan IV canted nozzle flow, even though the computer program, which has been developed under this study, is equally applicable to other odd-shaped, three-dimensional nozzle configurations.

II. Governing Equations

Normalized by the gas-phase stagnation state corresponding to the condition at the inlet plane, the governing equations written in weak conservative form for an unsteady, three-dimensional, two-phase flow are

$$\frac{\partial \boldsymbol{D}}{\partial t}+\frac{\partial \boldsymbol{E}}{\partial x}+\frac{\partial \boldsymbol{F}}{\partial r}+\frac{\partial \boldsymbol{G}}{\partial \theta}+\boldsymbol{H}=0$$

$$\boldsymbol{D}=\begin{bmatrix}\rho\\ \rho u\\ \rho v\\ \rho w\\ e\\ \rho_j(N-1)\\ \rho_j u_j(N-1)\\ \rho_j v_j(N-1)\\ \rho_j w_j(N-1)\\ h_j(N-1)\end{bmatrix},\qquad \boldsymbol{E}=\begin{bmatrix}\rho u\\ \tau p+\rho u^2\\ \rho uv\\ \rho uw\\ [e+(\gamma-1)p]\,u\\ \rho_j u_j(N-1)\\ \rho_j u_j^2(N-1)\\ \rho_j u_j v_j(N-1)\\ \rho_j u_j w_j(N-1)\\ h_j u_j(N-1)\end{bmatrix}$$

$$\boldsymbol{F}=\begin{bmatrix}\rho v\\ \rho uv\\ \tau p+\rho v^2\\ \rho vw\\ [e+(\gamma-1)p]\,v\\ \rho_j v_j(N-1)\\ \rho_j u_j v_j(N-1)\\ \rho_j v_j^2(N-1)\\ \rho_j v_j w_j(N-1)\\ h_j v_j(N-1)\end{bmatrix},\qquad \boldsymbol{G}=\frac{1}{r^{\delta}}\begin{bmatrix}\rho w\\ \rho uw\\ \rho vw\\ \tau p+\rho w^2\\ [e+(\gamma-1)p]\,w\\ \rho_j w_j(N-1)\\ \rho_j u_j w_j(N-1)\\ \rho_j v_j w_j(N-1)\\ \rho_j w_j^2(N-1)\\ h_j w_j(N-1)\end{bmatrix}$$

$$\boldsymbol{H}=\frac{\delta}{r^{\delta}}\begin{bmatrix}\rho v\\ \rho uv\\ \rho(v^2-w^2)\\ 2\rho vw\\ [e+(\gamma-1)p]\,v\\ \rho_j v_j(N-1)\\ \rho_j u_j v_j(N-1)\\ \rho_j(v_j^2-w_j^2)(N-1)\\ 2\rho_j v_j w_j(N-1)\\ h_j v_j(N-1)\end{bmatrix}+(N-1)\rho_j A_j\begin{bmatrix}0\\ (u-u_j)\\ (v-v_j)\\ (w-w_j)\\ B_j\\ 0\\ -(u-u_j)\\ -(v-v_j)\\ -(w-w_j)\\ -B_j\end{bmatrix} \tag{1}$$

with friction term

$$A_j=\frac{9}{2}\frac{\bar{\mu}_g f_j}{\bar{m}_j \bar{r}_j^2}\frac{\bar{L}}{\bar{V}_{\max 1}} \tag{2}$$

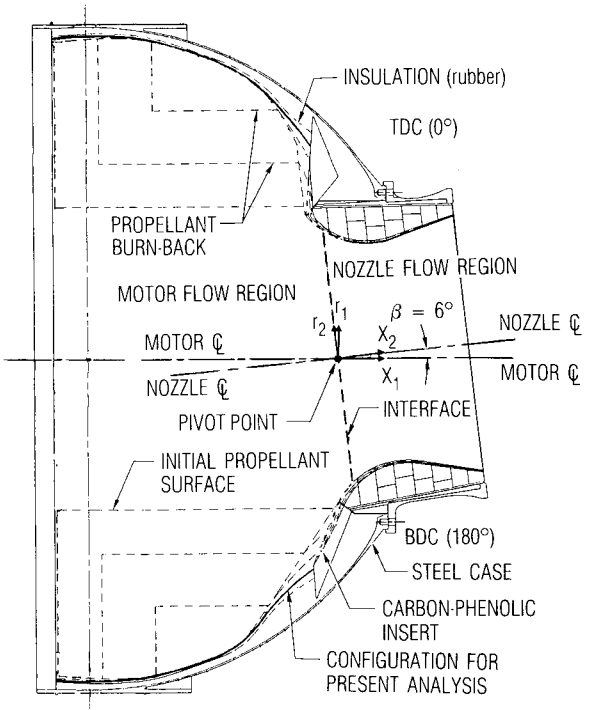

Fig. 1 Titan IV motor aft closure and nozzle configuration on the symmetry plane.

and energy exchange term

$$B_j=2\gamma[q_j\cdot\Delta q_j-g_c(T_j-T)-g_r(\epsilon_j T_j^4-\epsilon T^4)] \tag{3}$$

where

$$g_c=Nu_j/(6f_jP_r),\qquad g_r=\bar{\sigma}\bar{r}_j\bar{T}_{t1}^3/(3\bar{c}_p\bar{\mu}_g f_j)$$

$$q_j\cdot\Delta q_j=u_j(u-u_j)+v_j(v-v_j)+w_j(w-w_j)$$

$$T=P/\rho;\qquad T_j=[h_j/\gamma\rho_j-(u_j^2+v_j^2+w_j^2)]/\omega$$

The momentum transfer parameter f_j is defined as

$$f_j=C_D/C_{D_{\text{Stokes}}} \tag{4}$$

where C_D is the particle drag coefficient given in Ref. 11 and $C_{D_{\text{Stokes}}}=24/Re_j$.

The heat transfer parameter, namely the particle Nusselt number, is taken as[12]

$$Nu_j=2+0.459\,Re_j^{0.55}P_r^{0.33} \tag{5}$$

The particle Reynolds number is based on relative speed

$$|\Delta q_j|=\sqrt{(u-u_j)^2+(v-v_j)^2+(w-w_j)^2}$$

and is defined as follows:

$$Re_j=\frac{2|\Delta\bar{q}_j|\bar{r}_j\bar{\rho}}{\bar{\mu}_g}=2|\Delta q_j|\rho\frac{\bar{r}_j}{\bar{\mu}_g}\frac{1}{\tau}\frac{\bar{P}_{t1}}{\bar{V}_{\max 1}} \tag{6}$$

The gas viscosity is evaluated from

$$\bar{\mu}_g=\bar{\mu}_{t1}(\bar{T}/\bar{T}_{t1})^a \tag{7}$$

III. Three-Dimensional Transformations

From a general, three-dimensional, arbitrary configuration in the physical region (x,y,z), the one-to-one differentiable transformation to a rectangular grid with a uniform square mesh in the computational domain (ζ, ξ, η) shown in Fig. 2

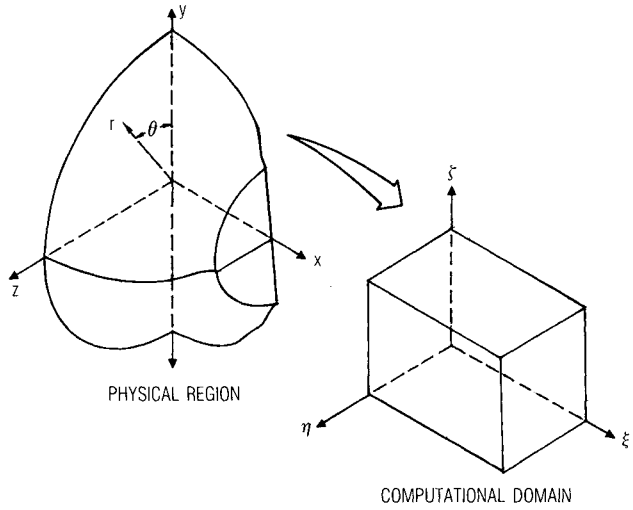

Fig. 2 Three-dimensional body-fitted coordinates transformation.

can be accomplished by using a three-dimensional, body-fitted, coordinate system developed in Refs. 9 and 10.

Formally applying the chain rule of change of independent variables for Eq. (1) results in the following conservation laws in the (ζ, ξ, η) space.

$$\frac{\partial D}{\partial t}+\frac{\partial E}{\partial \zeta}+\frac{\partial F}{\partial \xi}+\frac{\partial G}{\partial \eta}+H=0 \tag{8}$$

with

$$D = J_2 \boldsymbol{D}$$

$$E = C_{11}\boldsymbol{E} + C_{12}\boldsymbol{F} + C_{13}\boldsymbol{G}$$

$$F = C_{21}\boldsymbol{E} + C_{22}\boldsymbol{F} + C_{23}\boldsymbol{G}$$

$$G = C_{31}\boldsymbol{E} + C_{32}\boldsymbol{F} + C_{33}\boldsymbol{G}$$

$$H = J_2 \boldsymbol{H}$$

where the scale factors C_{ij} and the Jacobian of transformation J_2 are given in Ref. 13. Note that use of the Jacobian in a multidimensional transformation[14] eliminates the need to evaluate second-order partial derivatives for the scale factors of transformation. In the physical region described by the cylindrical coordinate system (x, r, θ), the independent variable y is replaced by r; z is replaced by θ in the scale factors and the Jacobian of transformation.

IV. Consideration of Nozzle Canting

The geometric transformation just described is applicable to a wide range of irregular, three-dimensional configurations with the same set of coordinate system for the motor chamber (hereafter referenced as "motor") and the nozzle. However, an added difficulty arises when the nozzle is canted or gimballed, which creates a different reference coordinate system for the nozzle from that for the motor. In a canted nozzle flow, the nozzle coordinate centerline is rotated an angle β from that of the motor centerline as shown in Fig. 1 for a Titan IV SRM aft closure configuration. Ambiguous interpretation of flow data ensues when only one set of the fixed reference coordinate system is adopted.

In this study, separate coordinate systems are used for the motor and nozzle flow regions. Two separate three-dimensional, body-fitted, coordinate systems utilizing the preceding transformation technique are generated for the motor and the nozzle. The interface between the two flow regions is taken to be a plane passing through the pivot point of canting and perpendicular to the nozzle centerline as shown in Fig. 1. The flows in the two regions are solved simultaneously. The treatment of flow variables at the interface needs special attention and is discussed later in this paper. In this way, confusion with the use of the motor or nozzle centerline as a reference coordinate centerline for a canted nozzle flowfield is eliminated. Precise interpretation of flow data can be obtained.

V. Solution Method

The weak conservative formulation [Eq. (8)] is a hyperbolic type with respect to the time variable in subsonic, transonic, and supersonic flow; it can be solved with the MacCormack finite difference scheme.[15] In the present study, the initial condition for one-phase flow is based on a one-dimensional isentropic assumption with the flow vector set to a local inclination angle from linear interpolation between the lower and upper wall along the same grid line (constant ζ, η line). The converged, one-phase results serve as an initial guess for the gas phase in the gas-particle, two-phase flow. Zero lag ($\lambda_q = \lambda_T = 1$) between the particle and gas phase is assumed initially to start the two-phase flow calculation.

The nozzle exit boundary condition is based on a linear extrapolation of conservative variables [$\boldsymbol{D}$ of Eq. (1)] since the flow is assumed to be supersonic at the nozzle exit plane, and any error generated from the extrapolation is not expected to propagate back and affect upstream results.

Two choices of inlet boundary conditions applied to the motor entrance region have been incorporated into the computer program. The first inlet boundary condition is obtained from an axisymmetric characteristics formulation similar to that discussed in Ref. 16 and used in Ref. 7. This boundary condition applies to an axisymmetric inlet flow but can be extended to a nonaxisymmetric, three-dimensional inlet flow.[17] The second inlet boundary condition corresponds to specified, fixed, flow variables at the inlet plane. Mach number, flow angles, and static pressure are specified on the inlet plane for one-phase flow. For two-phase flow, particle velocity lag (λ_q) and gas-to-particle temperature ratio (λ_T) are also needed on the inlet plane. This inlet boundary condition is suitable for a nonuniform flow at the inlet plane where flow variables can be obtained from experimental data or theoretical analyses. The theoretically correct inflow boundary is at the propellant burning surface, which requires that the computational region be extended all the way upstream to the forward closure and is beyond the scope of the present study.

For a cylindrical coordinate system, the conservative variables $\boldsymbol{G}$ and $\boldsymbol{H}$ in Eq. (1) at motor and nozzle centerlines are obtained from a linear extrapolation of the values at the interior points. In decoding conservative variable, $\boldsymbol{D}$, the flow variables at the motor and nozzle centerlines are obtained from interpolating the flow variables at one grid point above and at one grid point below the centerline on the symmetry plane. In a nonaxisymmetric nozzle, the radial velocity components at the coordinate centerline are not necessarily zero. On the symmetry plane for a canted nozzle, however, the meridional velocity components are zero. Therefore, at $\theta = 0$ at centerlines

$$v(1,k) = v(1,1)\cos\theta + w(1,1)\sin\theta$$

$$w(1,k) = -v(1,1)\sin\theta + w(1,1)\cos\theta$$

The indexes in parentheses indicate grid point indexes along r, θ directions on constant ζ planes. For generic three-dimensional flows, the meridional velocity on the symmetry plane is not necessarily zero, and a full 360 deg region needs to be considered.

The flow variables at the wall boundary are obtained from linear extrapolation of data from the adjacent interior points and then modified by the local tangency condition. A similar method is applied to the particle-phase velocity components; even though it is recognized that particles would interact with

the solid wall in a complicated manner, which accounts for enhanced motor and nozzle wall erosion. The particle-boundary interaction is a subject of further research.

On the interface plane of the motor and nozzle flow regions, the flow variables are evaluated from interpolating variables at upstream and downstream nodal points of the motor and nozzle interface, respectively. The scalar flow variables (pressure, density, temperature, and total energy) on the interface plane are invariant with respect to coordinate change from the motor to nozzle centerline and can be obtained directly from this interpolation process. The velocity vector, however, has different components on the interface for the motor and nozzle, respectively, and can be found from

$$\begin{cases} u_1 = \alpha_{11}u_2 + \alpha_{12}v_2 + \alpha_{13}w_2 \\ v_1 = \alpha_{21}u_2 + \alpha_{22}v_2 + \alpha_{23}w_2 \\ w_1 = \alpha_{31}u_2 + \alpha_{32}v_2 + \alpha_{33}w_2 \end{cases} \tag{9}$$

and

$$\begin{cases} u_2 = \alpha_{11}u_1 + \alpha_{21}v_1 + \alpha_{31}w_1 \\ v_2 = \alpha_{12}u_1 + \alpha_{22}v_1 + \alpha_{32}w_1 \\ w_2 = \alpha_{13}u_1 + \alpha_{23}v_1 + \alpha_{33}w_1 \end{cases} \tag{10}$$

For a nozzle with canting angle β, the direction cosines α_{ij} are

$$\alpha_{ij} = \begin{vmatrix} \cos\beta & -\sin\beta\cos\theta_2 & \sin\beta\sin\theta_2 \\ \sin\beta\cos\theta_1 & \cos\beta\cos\theta_1\cos\theta_2 + \sin\theta_1\sin\theta_2 & -\cos\beta\cos\theta_1\sin\theta_2 + \sin\theta_1\cos\theta_2 \\ -\sin\beta\sin\theta_1 & -\cos\beta\sin\theta_1\cos\theta_2 + \cos\theta_1\sin\theta_2 & \cos\beta\sin\theta_1\sin\theta_2 + \cos\theta_1\cos\theta_2 \end{vmatrix} \tag{11}$$

and the two coordinates are related by the following equations:

$$\begin{cases} \tan\theta_1 = \dfrac{r_2\sin\theta_2}{x_2\sin\beta + r_2\cos\beta\cos\theta_2} \\ r_1 = \dfrac{x_2\sin\beta + r_2\cos\beta\cos\theta_2}{\cos\theta_1} = \dfrac{r_2\sin\theta_2}{\sin\theta_1} \\ x_1 = x_2\cos\beta - r_2\sin\beta\cos\theta_2 \end{cases} \tag{12}$$

$$\begin{cases} \tan\theta_2 = \dfrac{r_1\sin\theta_1}{-x_1\sin\beta + r_1\cos\beta\cos\theta_1} \\ r_2 = \dfrac{-x_1\sin\beta + r_1\cos\beta\cos\theta_1}{\cos\theta_2} = \dfrac{r_1\sin\theta_1}{\sin\theta_2} \\ x_2 = x_1\cos\beta + r_1\sin\beta\cos\theta_1 \end{cases} \tag{13}$$

which also imply that uniform circumferential grid division in θ_2 (nozzle coordinates) will result in nonuniform circumferential grid division in θ_1 (motor coordinates) on the interface plane for a nozzle with nonzero canting angle.

Equation (9) is used to define the components of velocity vectors on the nozzle side with respect to the motor coordinates, and Eq. (10) is used to define the components of velocity vectors on the motor side with respect to the nozzle coordinates. The velocity components at the interface are found from interpolating the velocity components at the upstream and downstream grid points adjacent to the interface with a consistent reference (motor or nozzle) coordinate system. Additional descriptions of the boundary conditions and evaluation of interface flow variables are given in Ref. 13.

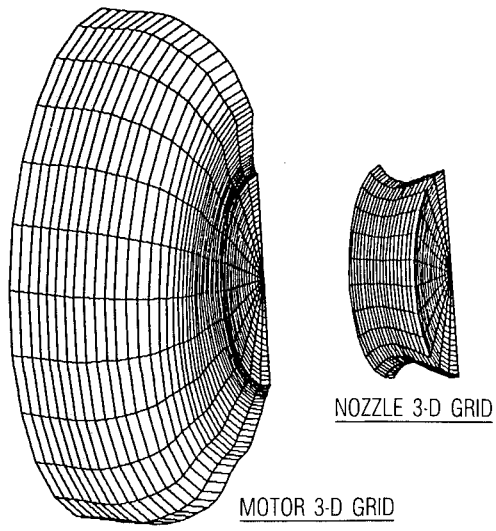

Fig. 3 Three-dimensional body-fitted coordinates grids for motor and nozzle.

VI. Three-Dimensional Body-Fitted Grids

The initial guess of three-dimensional, body-fitted grids for both motor and nozzle are based on linear interpolation from a specified boundary-nodal-points arrangement obtained from the two-dimensional, boundary-fitted coordinates transformation.[18] The inhomogeneous terms in the boundary-fitted coordinate transformation have been turned on to keep the streamwise grid lines near the nozzle wall in the concave region.

With the careful arrangement of boundary nodal meshes, fast convergence of iteration for the three-dimensional interior grid generation is assured. It is important that the inhomogeneous terms in the three-dimensional, body-fitted coordinate system for the interior nodal points generation be included, in order to be compatible with the two-dimensional, boundary-fitted coordinates specified on the three-dimensional grid boundaries for nodal points clustering control. An exponential decay function, similar to that in Ref. 18, is applied for the three-dimensional interior coordinate control. Numerical differentiation is then utilized to calculate the scale factors of transformation from an irregular, three-dimensional physical region to a uniformly divided, rectangular parallelepiped computational domain. The plots of the converged Titan IV SRM three-dimensional grids are shown in Fig. 3.

VII. One-Phase Cold Flow, $\gamma = 1.4$

To aid design and evaluation of the full-scale Titan IV SRM, a cold flow test with a 4.65% scale model was conducted.[19] Gaseous nitrogen ($\gamma = 1.4$) was introduced uniformly into the scaled motor chamber through sintered bronze porous surfaces to simulate propellant burning. This model provided test data for comparison with results from the present theoretical calculation.

In the one-phase cold flow ($\gamma = 1.4$) numerical study, the fixed nonuniform inflow condition is taken from the three-dimensional, cold-flow test data. The convergence criterion used in the transonic flow regime requires that the difference in mass flow rate and in Mach number on TDC, 90 deg, BDC,

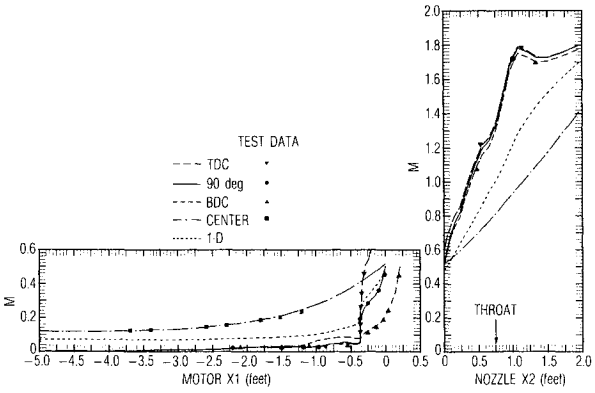

Fig. 4 Gas Mach number distributions (one-phase, $\gamma = 1.4$).

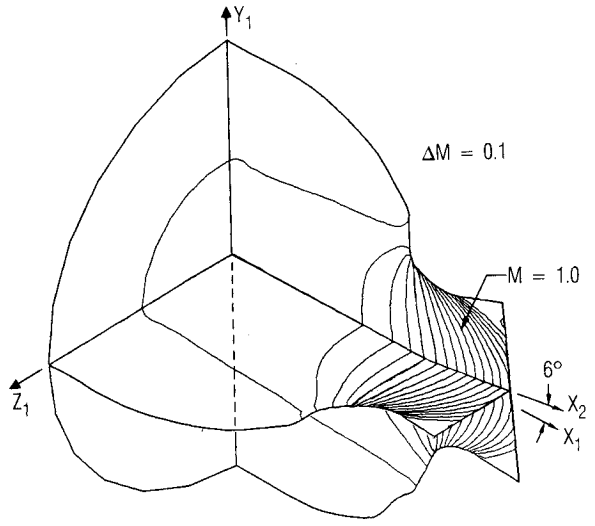

Fig. 5 Three-dimensional Mach number contour (one-phase, $\gamma = 1.4$).

and centerline at the nozzle throat be less than 0.001% for three consecutive time integration steps. The vectorized computer program—developed under this study with $40 \times 18 \times 13$ grid points in the motor and $20 \times 18 \times 13$ in the nozzle flow regions—takes up 1.1 million words memory on a CRAY X-MP14 supercomputer. The converged Titan IV one-phase, cold-flow transonic solution takes 2083 integration steps, which require 4 min, 54 s computation time. The computed three-dimensional nozzle, cold-flow discharge coefficient is 0.9855, based on a converged, three-dimensional gas mass flow rate of 2.997 lb/s and a one-dimensional, isentropic, gasmass flow rate of 3.041 lb/s at the nozzle throat for the 4.65% scale cold-flow model.

The Mach number distributions on the wall and along the centerlines are depicted in Fig. 4. It shows that, as flow approaches the motor-nozzle interface plane, a higher Mach number occurs on the TDC wall surface with a steeper slope change than that on the BDC wall surface. The computed Mach numbers at the throat are 1.339, 1.324, 1.293, and 0.813 at TDC, 90 deg, BDC, and centerline, respectively, for the cold flow with $\gamma = 1.4$. The results of a simple one-dimensional analysis at TDC + 90 deg plane are also shown in the figure for comparison. It clearly indicates the inadequacy of the one-dimensional analysis applied to a three-dimensional configuration. For the Titan IV nozzle, which is canted from BDC toward TDC, the higher pressure load associated with lower flow speed on the BDC plane than that on the TDC plane of the nozzle is to be expected. Shown on the same figure are the data obtained from the cold flow test.[19] In general, the results of the present three-dimensional flow analysis are in very good agreement with cold-flow test data; except in the low-speed compression corner region of the aft closure where the boundary layer is thick and viscous effects prevail.

An isometric projection of the three-dimensional Mach number contour plot is given in Fig. 5 for a clear visualization of the computed, overall three-dimensional flowfield. The sonic surface in the nozzle is marked in Fig. 5. This sonic condition is of particular interest to rocket nozzle designers, not only because it provides a "sonic barrier" beyond which an efficient supersonic marching scheme or method of characteristics is applicable and shock waves usually emerge, but also it is the state at which maximum convective heating occurs at the nozzle wall. Downstream of the sonic state, flow density and pressure decrease drastically and often result in reduced convective heating to the nozzle wall.

VIII. One-Phase Hot Flow, $\gamma = 1.19$

Based on the assumption that the measured cold-flow Mach number at the motor inlet plane is applicable to a full-scale hot firing, the one-phase numerical calculation for a combustion gas ($\gamma = 1.19$) at chamber temperature 5900°R and chamber pressure 570 psia (78.5 s into the burn) in the Titan IV SRM is also carried out. The converged Titan IV one-phase, hot-flow transonic solution takes 2168 integration steps, which require 5 min, 7 s computation time on a CRAY X-MP14 supercomputer. The computed three-dimensional nozzle, hot-flow discharge coefficient is 0.9850 based on a converged, three-dimensional gas mass flow rate of 3920.07 lb/s and a one-dimensional, isentropic gas mass flow rate of 3979.64 lb/s for the full-scale Titan IV motor with eroded throat diameter 3.3958 ft at 78.5 s into the burn. The computed Mach numbers at the throat are 1.305, 1.292, 1.266, and 0.824 at TDC, 90 deg, BDC, and centerline, respectively, for the hot flow with $\gamma = 1.19$.

Table 1 Titan IV two-phase-flow property data

Gas Phase
$\bar{C}_p = 2.68\ KJ/\text{kg} - °\text{K}$ (0.64 Btu/lb$_m$-°R)
$\bar{\mu}_{fl} = 8.88 \times 10^{-5}$Pa-s ($5.97 \times 10^{-5}lb_m$/ft-s)
$P_r = 0.45$
$a = 0.664$
$\gamma = 1.19$
Particle Phase
$\bar{C}_j = 1.38\ KJ/\text{kg} - °\text{K}$ (0.33 Btu/lb$_m$-°R)
$\bar{m}_j = 3203.69$ kg/m^3 (200 lb$_m$/ft^3)
$\phi = 28.8\%$
$\bar{r}_j = 6\bar{\mu}$

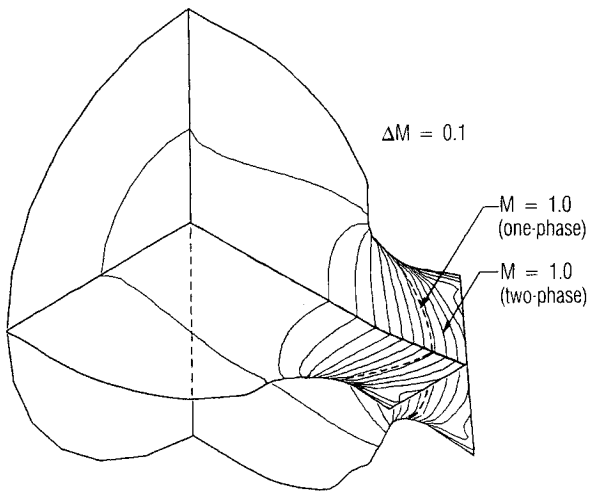

Fig. 6 Three-dimensional Mach number contour (two-phase, $\gamma = 1.19$).

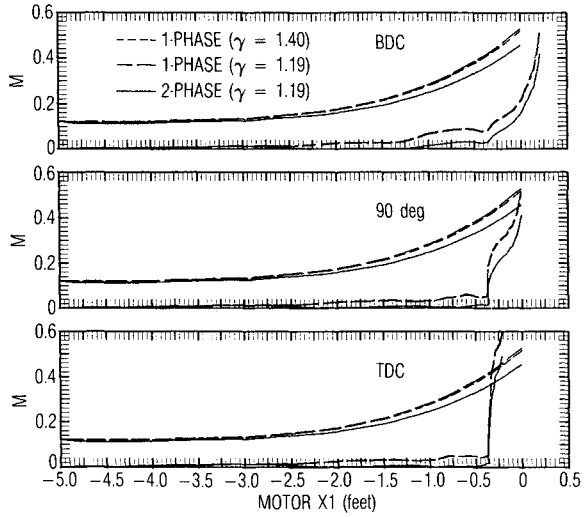

Fig. 7 Comparison of Mach number distributions (motor).

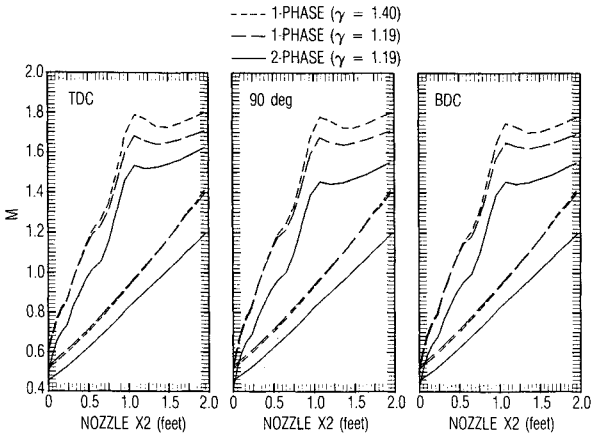

Fig. 8 Comparison of Mach number distributions (nozzle).

In general, the overall three-dimensional flow structure for the hot firing with $\gamma = 1.19$ is similar to that of the cold flow with $\gamma = 1.4$. Changing γ from 1.4 to 1.19 has the effect of decreasing the Mach number at supersonic speed and increasing the Mach number at subsonic speed. This follows the trend dictated by the one-dimensional isentropic theory.

IX. Two-Phase Hot Flow, Gas $\gamma = 1.19$

The two-phase flow property data for the Titan IV are shown in Table 1. For the two-phase hot flow with a single particle size of 6 $\bar{\mu}$ radius in the flowfield, the converged solution with a very small convergence criterion of 0.001% requires 5864 integration steps and 40 min computation time on a CRAY X-MP14 supercomputer. Increasing the convergence criterion to 0.005% will significantly reduce the required computation time to less than 10 min. The discharge coefficient is found to be 1.1764 based on a computed, three-dimensional total mass flow rate 4681.59 lb/s (gas phase 3348.29 lb/s + particle phase 1333.30 lb/s) and a one-dimensional, isentropic gas mass flow rate 3979.64 lb/s. The discharge coefficient is >1 when a two-phase mass flow rate is compared with a one-dimensional, gas mass flow rate. The computed gas-phase Mach numbers at the throat are 1.152, 1.096, 1.092, and 0.721 at TDC, 90 deg, BDC, and centerline, respectively, for the two-phase, hot flow. The gas-phase Mach number contours for the two-phase, hot flow are given in Fig. 6 where the sonic surfaces for both one- and two-phase flows are shown for comparison. With the presence of particles in the flow region, gas-phase expansion is slowed down significantly.

Figures 7–10 summarize and compare the Mach number and pressure distribution on the wall and centerlines of the motor and nozzle flow region for one-phase cold flow, one-phase hot flow, and two-phase hot flow. Although the difference in flow variables between the one-phase cold flow ($\gamma = 1.4$) and the hot flow ($\gamma = 1.19$) is negligible in the low subsonic motor flow region, it cannot be ignored in the transonic and supersonic nozzle flow region. The difference is more pronounced when the particles are introduced into the flow. A higher pressure load on the nozzle wall from the two-phase hot flow than that from the one-phase cold flow is evident from the analysis results.

For a giant Titan IV motor (10 ft diameter, 113 ft long), it is important to have accurate information on total pressure drop from the forward end of the motor to the aft closure. In a motor firing test, the forward end pressure can be conveniently measured (usually through the igniter boss). But aft closure total pressure is usually unknown; even though it is the aft closure total pressure that directly affects performance of a motor, especially during ground level vehicle liftoff. In this regard, if static pressure in the liquid injection thrust vector control (LITVC) ports, located in the exit cone downstream of the nozzle throat, is monitored during full-scale Titan IV static tests, the present numerical calculation can be iteratively applied for defining the aft closure total pressure. With an assumed aft closure total pressure at the motor inlet plane, the

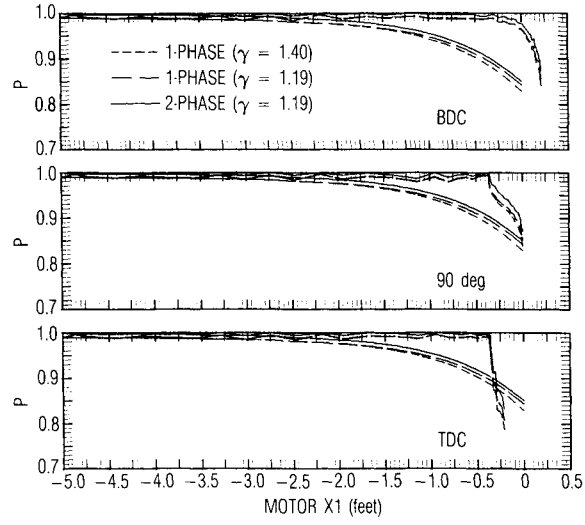

Fig. 9 Comparison of pressure distributions (motor).

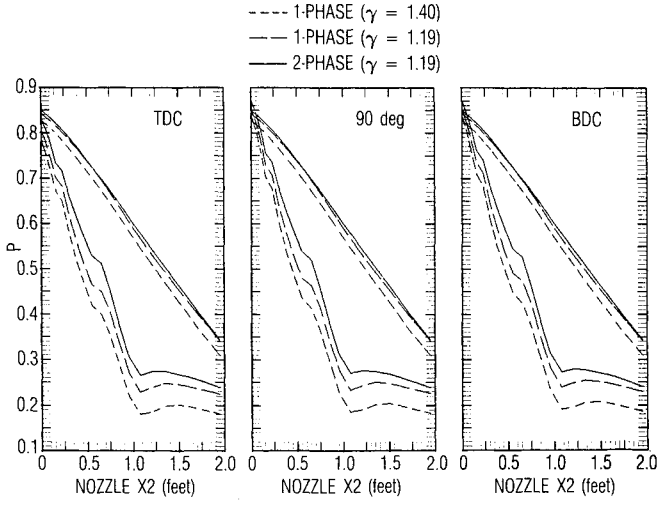

Fig. 10 Comparison of pressure distributions (nozzle).

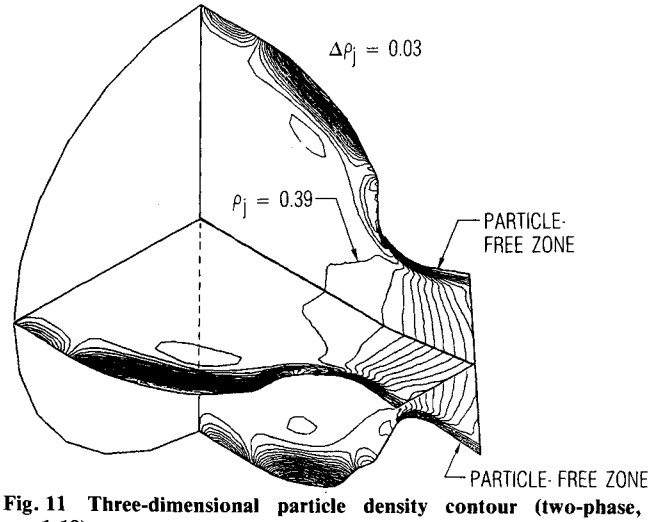

Fig. 11 Three-dimensional particle density contour (two-phase, $\gamma = 1.19$).

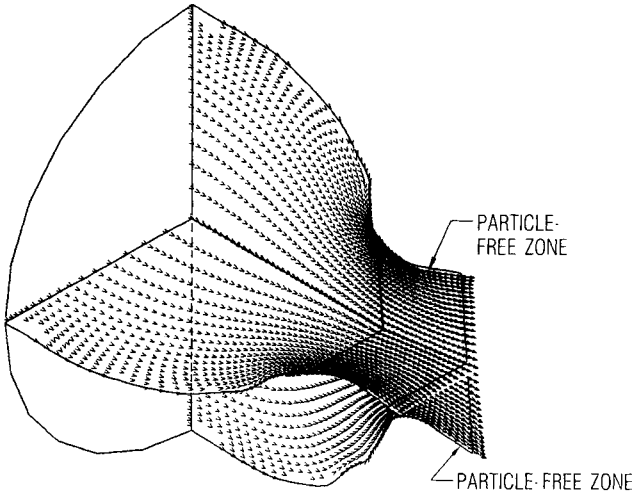

Fig. 12 Three-dimensional particle velocity vectors (two-phase, $\gamma = 1.19$).

application of the present numerical method will result in calculated static pressure at the LITVC ports, which is not expected to agree with that obtained from measurement. Adjusting the aft closure total pressure until the calculated static pressure at the LITVC ports agrees with the measured value will then establish the aft closure total pressure field.

The three-dimensional feature of two-phase flow in the Titan IV SRM is portrayed in the particle density contours and particle velocity vector plots of Figs. 11 and 12. Since a particle flow path cannot faithfully follow a steep change in wall slope, particles are clustered near the wall with a steep entrance angle. A distinctive, particle-free zone appears in the calculated results. On the TDC wall with a steep-slope change, the particle-free zone occurs upstream of the throat. On the BDC wall, with a gradual slop change, the particle-free zone occurs downstream of the throat. Moreover, since heavy particles cannot effectively turn around the corner of the nozzle entrance wall with a steep-slope change and tend to cluster near the centerline of the nozzle, significant reduction in gas-phase velocity in the two-phase flow from that in the one-phase flow at the centerline near the nozzle exit plane is observed.

The particle velocity lag λ_q and gas-to-particle temperature ratio λ_T on nozzle throat plane and nozzle exit plane are given in Fig. 13. On nozzle throat plane, λ_q and λ_T are higher at the centerline than those near the wall. On nozzle exit plane, the reverse is true because of gas-phase recompression near the wall downstream of the throat. Clustering of particles near the nozzle centerline downstream of the throat also causes reduction in gas-phase speed, which results in a slight increase of λ_q from nozzle throat to exit plane.

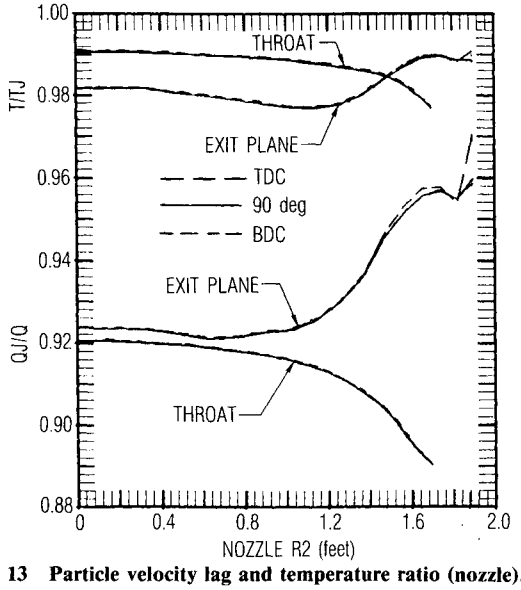

Fig. 13 Particle velocity lag and temperature ratio (nozzle).

The particle-phase flowfields presented in Figs. 11 through 13 are useful to rocket nozzle designers for particle impact erosion calculations. Adequate insulation design without undue weight penalty is important to vehicle survivability in a hostile launching environment. An investigation of enhanced insulation erosion from particle impact usually requires knowledge of incident particle density, flow angle, and velocity. This information can be obtained directly from a fully coupled, two-phase analysis such as the one shown in this paper.

X. Conclusions

In this study, the treatment of complicated, three-dimensional motor and nozzle geometries is facilitated through use of three-dimensional, body-fitted grid systems. Difficulty and confusion associated with a canted nozzle are eliminated through introduction of multiple flow regions, which allow precise interpretation of flow variables in each region. The idealized, fully coupled, gas-particle, two-phase flow governing equations in three-dimensional space are solved numerically. Cold flow test data are utilized for verification of the operational computer program. Results of the analysis are presented for a rocket motor of practical importance in space exploration. The groundwork laid herein will be helpful to further study of viscous, three-dimensional, multiparticle sized, two-phase nozzle flows.

References

[1]"Three-Dimensional Computation Techniques Applied to Internal Flows in Propulsion Systems," AGARD Lecture Series No. 140, May 1985.

[2]Kliegel, J. R., "One-Dimensional Flow of a Gas Particle System," Institute of Aeronautical Sciences, New York, IAS Paper 60-5, Jan. 1960.

[3]Bailey, W. S., Nilson, E. N., Serra, R. A., and Zupnik, T. F., "Gas Particle Flow in an Axisymmetric Nozzle," *ARS Journal,* June 1961, pp. 793-798.

[4]Kliegel, J. R., "Gas Particle Nozzle Flows," *Ninth (International) Symposium on Combustion,* Academic, New York, 1963, p. 811.

[5]Regan, J. F., Thompson, H. D., and Hogland, R. F., "Two-Dimensional Analysis of Transonic Gas-Particle Flows in Axisymmetric Nozzles," *Journal of Spacecraft and Rockets,* Vol. 8, 1971, pp. 346-351.

[6]Rudinger, G., "Flow of Solid Particles in Gases," AGARD-AG-222, Oct. 1976.

[7]Chang, I-S., "One- and Two-Phase Nozzle Flows," *AIAA Journal,* Vol. 18, Dec. 1980, pp. 1455-1461; also AIAA Paper 80-0272.

[8]Chang, I-S., "Three-Dimensional, Two-Phase Supersonic Nozzle Flows," *AIAA Journal,* Vol. 21, May 1983, pp. 671–678; also AIAA Paper 81-1219.

[9]Mastin, C. W., and Thompson, J. F., "Transformation of Three-Dimensional Regions onto Rectangular Regions by Elliptic Systems," *Numerische Mathematik,* Springer-Verlag, New York, Vol. 29, 1978, pp. 397–407; also Institute for Computer Applications in Science and Engineering, ICASE Rept. 76-13, Hampton, VA, April 1976.

[10]Mastin, C. W. and Thompson, J. F., "Three-Dimensional Body-Fitted Coordinate Systems for Numerical Solution of the Navier-Stokes Equations," AIAA Paper 78-1147, July 1978.

[11]Henderson C. B., "Drag Coefficients of Spheres in Continuum and Rarefield Flows," *AIAA Journal,* Vol. 14, June 1976, p. 707.

[12]Carlson, D. J., and Hogland, R. F., "Particle Drag and Heat Transfer in Rocket Nozzles," *AIAA Journal,* Vol. 2, Nov. 1964, p. 1980.

[13]Chang, I-S., "Three-Dimensional, Two-Phase, Transonic, Canted Nozzle Flows," AIAA Paper 88-3201, July 1988; also Aerospace Corp., El Segundo, CA, Rept. TR-0089 (4530-04)-1, Dec. 1988.

[14]Viviand, H., "Formes Conservatives des Equations de la Dynamique des Gaz," *La Recherche Aerospatiale, Annee 1974,* Vol. 1, Jan.-Feb. 1968, p. 65.

[15]MacCormack, R. W., "The Effect of Viscosity in Hyper Velocity Impact Cratering," AIAA Paper 69-354, May 1969.

[16]Serra, R. A., "Determination of Internal Gas Flows by a Transient Numerical Technique," *AIAA Journal,* Vol. 10, May 1972, pp. 603–611.

[17]Phares, W. J., "Computation of Three-Dimensional Transonic Internal Flow in Cylindrical Coordinates," Arnold Engineering Development Center, Tullahoma, TN, AEDC-TR-80-56, Aug. 1981.

[18]Thompson, J. F., Thames, F. C., and Mastin, C. W., "Boundary-Fitted Curvilinear Coordinates Systems for Solution of Partial Differential Equations on Fields Containing Any Number of Arbitrary Two-Dimensional Bodies," NASA CR2729, July 1977; also *Journal of Computational Physics,* Vol. 24, 1977, pp. 245–273.

[19]Dunlap, R., et al., "Titan IV (CELV/T34D7) Cold Flow Study Report," Chemical Systems Division, United Technologies Center, CSD4001-86-89, San Jose, CA, July 1986.